

711-39

199055

50R

TECHNICAL NOTE

D-429

CREEP BENDING AND BUCKLING OF THIN

CIRCULAR CYLINDRICAL SHELLS

By Burton Erickson, Francis W. French, Sharad A. Patel,
N. J. Hoff, and Joseph Kempner

Polytechnic Institute of Brooklyn

NATIONAL AERONAUTICS AND SPACE ADMINISTRATION
WASHINGTON

June 1960

(NASA-TN-D-429) CREEP BENDING AND BUCKLING
OF THIN CIRCULAR CYLINDRICAL SHELLS
(Polytechnic Inst. of Brooklyn) 50 p

N89-70957

Unclas
00/39 0199055

NATIONAL AERONAUTICS AND SPACE ADMINISTRATION

TECHNICAL NOTE D-429

CREEP BENDING AND BUCKLING OF THIN

CIRCULAR CYLINDRICAL SHELLS

By Burton Erickson, Francis W. French, Sharad A. Patel,
N. J. Hoff, and Joseph Kempner

SUMMARY

A number of circular cylindrical shells manufactured of 5052-O aluminum alloy were tested in pure bending, most at a temperature of 500° F, but a few at room temperature. Fifty-four specimens were unreinforced, seventeen had longitudinal, fifteen had circumferential, and sixteen had longitudinal and circumferential reinforcing elements. All the specimens not subjected to static tests failed by creep buckling. The results of the experiments are presented in tables and diagrams. A few theoretical considerations are given in an appendix.

INTRODUCTION

When a structural element is simultaneously subjected to an elevated temperature and a load, it is observed that the element deforms in the familiar elastic or elastoplastic manner at first. Further observation shows, however, that additional deformations occur which continue with time even though the load is constant. These time-dependent deformations are known as creep deformations.

For many types of structural elements, the creep deformations eventually accelerate and cause a failure which is similar to the elastic buckling failure that occurs at room temperature; this type of failure is known as creep buckling. The interval of time that elapses between the application of the load and the collapse of the structure is then known as the critical or buckling time.

The importance of creep research in general is a consequence of the rapid developments made in high-speed flight in the last decade. It is now a well-known fact that when an aircraft, missile, or rocket flies at supersonic speeds its surface is heated by the airstream. One can imagine that if this heating is applied to the surface for a sufficient length of time, large portions of the structure will be elevated in temperature. If some of these portions of the structure are simultaneously

stressed, creep effects may become important. Creep may adversely affect the strength of a structure by changing the stress distribution. Creep may also cause large deformations of the structure which can render it unserviceable. For these reasons it is important to the aircraft designer or structural engineer to have information regarding the creep behavior of various types of structural materials and structural elements.

The behavior of the simpler types of structural elements such as beams, columns, and frames has been investigated both theoretically and experimentally. The present report is concerned with the creep behavior of a more complex type of structure, a cylindrical shell loaded by end moments. This problem is of interest to the aeronautical engineer since it involves a type of structure often found in aircraft.

Experiments were performed on 102 thin-walled circular cylindrical shells which were subjected to pure moment loadings at elevated temperature and at room temperature. The primary objective of the experiments was to determine the influence of changes in the ratio of skin thickness to cylinder diameter, and the effect of the number and placement of reinforcements on time to failure in creep buckling. The effect of cylinder length was also briefly investigated. Results of the experiments are presented in the form of curves and tables. The experimental apparatus was designed and constructed specifically for this testing program and it is described in detail in reference 1. A total of 14 different types of specimens was tested; detailed specifications for each type are listed in table 1.

A theory for predicting the creep-buckling time of thin circular cylindrical shells has been developed by Hoff (ref. 2). This theory is based upon the supposition that the cylinder collapses by flattening. In order to predict the critical time by use of this theory, it is necessary to solve two simultaneous differential equations numerically. The appendix to the present report describes a simplification, based on experimental observations, which enables one to calculate the creep-buckling time by means of a simple integration. The results of this simplified method are compared with those from the method of Hoff as well as with results of experiments in numerical examples.

Determination of the creep-buckling time by either the method of reference 2 or the simplified method requires first finding the initial elastic values of curvature of the cylinder axis and the flattening ratio of the cylinder cross section. A simplification of the method of reference 2 for calculating these elastic quantities and the effect of instantaneous inelastic behavior of the material on the creep-buckling time are also discussed in the appendix.

This report is a summary of the results of an investigation which has been partially reported in references 1 and 3. The investigation

was carried out at the Polytechnic Institute of Brooklyn under the sponsorship and with the financial assistance of the National Advisory Committee for Aeronautics. The authors wish to thank Mr. Samuel Lederman for his work in designing the electrical system which formed the basis for the experimental equipment used.

SYMBOLS

a	cylinder flattening
C, C_1, C_2	simplifying terms, see appendix
d_1, d_2, d_3	deflections of end of cantilever beam; see figure 7
e	interaction factor used in calculating elastic curvature and elastic flattening
E	Young's modulus
h	cylinder wall thickness
h_b, h_e	cylinder wall thicknesses effective in resisting bending and axial extension, respectively
I	moment of inertia of cylinder cross section with respect to the horizontal centroidal axis
J_{1n}, J_{1p}, J_3, J_5	constants dependent upon n and p
L, l_1, l_2	lengths of deflection-measuring equipment shown in figure 7
L_1	length of cylinder
M	bending moment
n, p	creep exponents
r	radius of cylinder
T	parameter dependent upon h_e , h_b , and r
t	time

\bar{t}	nondimensionalized time parameter, $\kappa_{av}t/\kappa_0$
y	distance from neutral axis
α	flattening ratio, a/r
$\bar{\alpha}$	flattening ratio parameter, α/C_2
β	axial displacement of point of intersection of the axis with the end plane of the cylinder
δ	vertical displacement of point of intersection of the axis with the end plane of the cylinder
ΔD	change in length of vertical diameter of cylinder
ϵ	bending strain
η	ratio of average curvature rate to steady curvature rate
θ	rotation of cylinder end plane
κ	curvature of cylinder axis
κ_1	elastic curvature of cylinder axis obtained from simple beam theory
λ	creep constant in extension
μ, μ'	creep constants in bending
ρ	radius of curvature of cylinder axis
σ	bending stress
ψ	angle measured from horizontal in plane perpendicular to axis of cylinder
$(\dot{})$	derivative with respect to time or rate

Subscripts:

av	average
cr	critical

max	maximum
r	reduced
s	steady
o	elastic or initial

TEST APPARATUS AND PROCEDURE

Apparatus

The main parts of the test apparatus were a lever loading mechanism designed to maintain a constant bending moment on the cylinder (fig. 1), a rigid support for the cylinder (figs. 2 and 3), and an oven capable of producing a constant elevated temperature in the cylinder throughout the range of 150° to 1,000° F within a tolerance of $\pm 3^\circ$ F (figs. 4 to 6). The pure bending moment applied to the cylinder was the weight suspended from the apex of the loading triangle multiplied by the distance from the apex to the pivot in the middle of the base of the triangle (fig. 1) plus the weight of the loading triangle multiplied by the distance of its center of gravity from the pivot. The apparatus is described in detail in reference 1.

Measurement of Temperature

Temperatures were measured at 20 points on the specimen. Iron-constantan thermocouples were fastened to the specimen with heat-resistant tape in such a manner as to insure that the junctions remained in close contact with the surface at all times. The thermocouples were wired to a selector switch connected to a No. 1117 Brown indicating potentiometer. The temperatures at the 20 points were read consecutively.

Of the points surveyed, four were at each extreme end of the cylinder, four at one-quarter length, four halfway between the ends, and four at three-quarter length. In each of the planes one thermocouple was located at the top, one at the bottom, and one on each end of the horizontal diameter of the cylinder. The control points for automatic temperature regulation were coincident with the survey points halfway between the ends.

Measurement of Deformations

The deformations measured were:

- (1) Rotation of the end plane of the cylinder θ
- (2) Vertical displacement of the point of intersection of the axis of the cylinder with end plane δ
- (3) Axial displacement of the point of intersection of the axis of the cylinder with the end plane β
- (4) Change in vertical diameter in a plane perpendicular to the axis of the cylinder and bisecting the cylinder ΔD

For measurement of the first three of these deflections, the loading linkage was used to transmit the motion of points in the end plane of the cylinder to the outside of the oven where measurements could be made at room temperature. Measurements were made by using cantilever-beam transducers and SR-4 Type M indicators; the cylinder deflections were obtained from the geometry of the system (fig. 7). In each particular case this was done as follows.

To measure θ , one end of a cantilever beam of length l_1 was clamped in a vertical position to the upright of the castored base plate that acted as fulcrum for the counterbalancing beam. The other end of the cantilever was set against the base of the loading triangle. From the geometry of the linkage it is seen that

$$\frac{d_1}{l_1} = \tan \theta \approx \theta \quad (1)$$

where d_1 is the deflection of the end of the cantilever beam.

To determine δ , one end of a cantilever beam of length l_2 was clamped in a horizontal position to the upright of the base plate. The other end of the cantilever was set against the counterbalancing beam. From the geometry it is seen that

$$\delta = (L/l_2)d_2 \quad (2)$$

where d_2 is the deflection of the end of the cantilever and L is the length of the counterbalancing beam from the fulcrum to the center of the cylinder end plane.

For determining β , one end of a cantilever beam was bolted to the supporting structure on which the base plate rests. The other end was set against the edge of the castored base plate. In this case

$$\beta = d_3 \quad (3)$$

where d_3 is the deflection of the end of the cantilever.

Measurements made in the first few experiments indicated that the magnitude of β was small compared with that of θ and δ , and in subsequent tests only the latter two quantities were measured.

The change in diameter in the elevated-temperature tests was measured by means of a high-temperature linear variable differential transformer made by Schaevitz Engineering Co. of Camden, New Jersey. The stationary transformer coil was suspended from the upper surface inside the cylinder. A long slender rod was attached to the transformer core which was placed inside the coil with the end of the rod resting on the bottom surface of the cylinder, so that the assembly could move freely in a vertical direction. Relative motion between the core and coil as a result of the cylinder flattening changed the output of the transformer. The change in output voltage was calibrated as a measure of change in diameter. A graphical record of diameter change with time was obtained with the aid of a Brown "Electronik" recorder made by the Minneapolis-Honeywell Regulator Co. In one of the room-temperature static tests, the change in diameter was measured by another means. A dial gage set in a measuring fixture was used, the fixture being designed so that one end of the vertical diameter of the cylinder was in contact with the fixture itself and the other end was in contact with the spring-loaded plunger of the dial gage. By keeping the cylinder in contact with the fixture as the load was applied, change in the vertical diameter could be read on the dial gage.

Many difficulties were encountered in measuring diameter change of cylinders at elevated temperatures. Calibration of the transformer was awkward and stabilization of the recorder proved troublesome. Because of these difficulties, the change in diameter was measured in comparatively few experiments and the accuracy of the measurement was not up to the standard of that of the other deformation measurements.

Specimens

All specimens, both reinforced and unreinforced, were made of 5052-0 aluminum-alloy sheet with thicknesses of 0.032, 0.040, 0.051, or 0.064 inch. The sheet was rolled into a cylinder 16 inches in diameter and 48 or 38 inches long with a $1\frac{1}{4}$ -inch overlap at the end of juncture.

AN430-AD4 rivets spaced 1/2 inch apart closed the cylinder. Longitudinal reinforcement consisted of extruded bars attached around the circumference to the inside of the cylindrical shell. These longitudinal stiffeners were made of solid rectangular 5052-0 aluminum alloy of 1/2- by 1/4-inch cross section with the 1/2-inch side against the sheet. Each stiffener was riveted to the sheet with AN430-AD4 rivets at 1/2-inch spacing.

Circumferential reinforcement consisted of equally spaced rings along the length of the cylinder. These rings were of 1/2- by 1/4-inch or 1/2- by 1/8-inch rectangular cross section with the 1/2-inch side against the sheet. The rings were rolled to a 16-inch inside diameter from extruded 5052-0 or 2024-T4 stock and fastened to the outside of the cylinders by sixteen 6-32 steel bolts or by AN430-AD4 rivets at 1-inch spacings.

The decision of which aluminum alloy to use for the specimens was made on the basis of past experience. Creep experiments at the Polytechnic Institute of Brooklyn have shown that the material properties of the 5052-0 alloy, in contrast with those of some aluminum alloys more commonly used for structures, do not change significantly with time because of soaking at elevated temperature. It was felt that the use of an unstable, although structurally more interesting, material would add an unwanted complication to the investigation at this time. In one instance, however, 2024-T4 extruded stock was used for ring reinforcements because 5052-0 alloy was not available at the time (see table 1).

Steel clamping rings with a 16-inch inside diameter, 1-inch thickness and 4-inch length, having 1/2- by $2\frac{3}{4}$ -inch flanged ends slipped over the ends of the cylinder. Two circumferential rows of 5/8-inch-diameter holes $1\frac{1}{4}$ and 3 inches from the end of the ring were provided to take through bolts for drawing 24 knurled-faced convex clamps in two rows against the inside surface of the cylinder, and in this manner to secure 4 inches of the end of the cylinder within a steel ring at each end. The unsupported length of the cylinder was then either 40 or 30 inches.

The flanged portion of the rear clamping ring contained a circumferential set of holes which were matched to studs protruding from the strongback. The ring was secured in place on these studs.

The load links and counterbalance beam were attached to a vertical fitting consisting of two steel bars $1/2$ inch by 3 by 21 inches spaced $1\frac{1}{4}$ inches apart and welded to the front face of the front clamping ring across the entire diameter (fig. 2). The loading links were pinned to the ends of the fitting by 1-inch-diameter hardened steel pins; the counterbalancing beam was similarly pinned at the midpoint. The center-to-center spacing of the end holes was 18 inches; the third hole was exactly halfway between the ends.

Procedure

With the test specimen securely mounted the thermocouples were attached, the clamping-ring heaters were positioned and connected, and the oven was rolled into place around the specimen and sealed. The load links were connected to the lever, and the counterbalancing beam was pinned and weighted. A hydraulic jack was used to support the end of the loading lever, and the deadweight load was applied. At this stage, the entire weight was supported by the jack.

Switches were thrown and full power was fed to all heaters. As the temperature of the oven increased, a careful check was maintained at each of the 20 instrumented points. Some points naturally approached the test temperature more quickly than others. When the test temperature was reached at these points, the corresponding heaters were cut back to maintain it. Stabilized test temperature was reached in $1\frac{1}{4}$ hours and was maintained therefrom with a maximum variation of $\pm 3^{\circ}$ F for the remainder of the test.

When the temperature was stabilized, the load was applied. This was accomplished by opening the metering valve of the hydraulic jack and allowing the full load to be smoothly transferred from the jack to the end of the lever. The operation took about 10 seconds. The time to failure of the cylinder was measured from the instant of full load application.

In addition to creep-buckling experiments, static-buckling tests were also performed to obtain the instantaneous failure load of the specimen. These tests were carried out at both room and elevated temperatures. Load was applied by a hydraulic jack. A dynamometer was attached to the loading triangle and connected to an indicator. As the load was increased from zero, the indicator was continuously nulled and the maximum strain reading, corresponding to the buckling load, was noted. In cold static tests, the load could be increased at a leisurely rate and nulling the indicator was no problem. In hot static tests, however, it was necessary to apply load rapidly in order to avoid creep deformations;

consequently, the nulling proved a problem. For this reason the Brown "Elektronik" recorder was used to measure the buckling load.

TEST RESULTS

The principal results of the 102 experiments are summarized in tables 1 and 2. Figure 8 shows plots of applied bending moment versus critical time for the test cylinders; curves are faired through the different points. Test results for both the reinforced and unreinforced cylinders are shown in the figure.

All cylinders tested failed by buckling on the compression side. Unreinforced cylinders developed multilobed buckles in reasonable approximation to a diamond pattern and with reasonably consistent wave lengths. Reinforced cylinders, excepting those with only circumferential reinforcement, failed by general instability. Here again, the buckling pattern was multilobed and generally consistent. Specimens reinforced with 7 circumferential rings developed a multilobed pattern but failed due to panel instability. Specimens with 19 rings developed single intrabay accordion pleats and failed because of panel instability. Figures 2 and 9 are photographs which are representative of the various types of failures. Figure 10 presents curves of deflection versus time obtained from experiments on reinforced and unreinforced cylinders. The slope of the straight portion of the curve of end rotation versus time was obtained for each test and designated as $\dot{\theta}_S$. The assumption was made that the longitudinal axis of the cylinder deflected into a circular arc under loading so that

$$\kappa = \frac{\theta}{L_1} \quad (4)$$

where κ was the curvature of the cylinder axis and L_1 was the length of the cylinder. The steady curvature rate corresponding to the steady end-rotation rate was obtained as:

$$\dot{\kappa}_S = \frac{\dot{\theta}_S}{L_1} \quad (5)$$

The bending moment was plotted against the steady curvature rate on a double logarithmic scale (fig. 11) for various types of specimens. The apparatus for measuring deflections was developed after the 0.064-inch unreinforced cylinders had been tested so that it was not possible to

make a similar plot for this type of specimen. The plots of figure 11 indicated that, for each type of specimen, a straight line could be passed through the points without an undue amount of scatter. This implied that the moment was related to the steady curvature rate as

$$\dot{\kappa}_S = (M/\mu')^n \quad (6)$$

where M is the bending moment and μ' and n are constants. The values of μ' and n as determined from figure 11 were collected and presented in table 3.

Discussion

Figure 8 is a composite plot of bending moment against critical time for all cylinders tested. From this figure and table 3, the following general information may be extracted.

Unreinforced cylinders.- The bending moment required to cause creep buckling at a specified time is increased if the thickness of sheet is increased. A qualitative idea of the influence of sheet thickness on required bending moment is obtained if these quantities are plotted for different values of the critical time. This cross plot is shown by the unbroken straight-line portion of the curves in figure 12 and indicates that, within the range of sheet thicknesses tested, the bending moment is proportional to the sheet thickness for a given value of the critical time.

Longitudinally reinforced cylinders.- Figure 8 shows that the addition of longitudinal reinforcing elements materially increases the creep buckling strength of the basic shell. This can be seen by comparing the curves marked C and G (representing two types of longitudinally reinforced specimens) with the curve of the 0.051-inch-thick basic shell. One may obtain an idea of the increase in strength, relative to an unreinforced cylinder, if use is made of the concept of effective thickness. One imagines that the total stringer cross-sectional area is spread over the entire circumference of the shell and the resulting thickness is added to the sheet thickness; in the case of types C and G specimens, the effective thicknesses are 0.091 and 0.081 inch, respectively. The bending moments required to cause creep buckling at specified values of the critical time are obtained from the C and G curves of figure 8 and are plotted in figure 12. By extrapolating the curves of figure 12 it is seen that for a given critical time the bending moment required to buckle an unreinforced cylinder of 0.091- or 0.081-inch thickness is greater than that

required to buckle a longitudinally reinforced cylinder of a corresponding effective thickness. This limited evidence may be taken to imply that for a given cross-sectional area, or for a given weight of structure, an unreinforced cylinder is stronger in creep bending than a longitudinally reinforced cylinder. It should be stressed that this conclusion is merely tentative as it is based on test results obtained from only two series of longitudinally reinforced cylinders. It should further be noted that the type of stringer cross section used in the test is an inefficient one and that the use of a more efficient type of stringer might lead to different results.

Circumferentially reinforced cylinders.- Specimens reinforced with rings alone, even at very close spacing, were no stronger in bending than those without rings. This may be seen in figure 8, where the test points for the ring-reinforced specimens of types H and I plot within the scatter band of the 0.051-inch unreinforced series. These tests covered only two isolated possibilities of combinations of ring spacing and cross section, but it seems reasonable to surmise that circumferential reinforcement in any case would be inefficient in the presence of moment loading.

Circumferentially and longitudinally reinforced cylinders.- When rings act in combination with stringers, the strength of the cylinder is increased over that obtained with only stringer reinforcement. This may be seen in figure 8 by comparing curves G and J with curves C and F. While adding rings to a longitudinally reinforced cylinder does increase the strength, it does so at a disproportionate increase in weight.

Effect of length.- There appears to be no distinct influence of length on buckling strength in the range of these tests. Experimental points for unreinforced cylinders of 0.051-inch sheet thickness and both 40- and 30-inch lengths all fall within the scatter band for both series. It should be noted, however, that the lengths considered are not significantly different.

The effect of length on the creep constants defined by equation (6) may be seen in figure 11(b), where a single straight line may be passed through test points for both 30- and 40-inch lengths without an undue amount of scatter. This line yields a value for n of 5.0 as compared to the value 5.8, which is obtained by considering only the 40-inch-length test points. This then strengthens the conclusion that the effect of length on the creep properties is unimportant in this length range. It should also be noted that the test points for the specimens reinforced with type I rings in figure 11(b) fall within the scatter band of the 0.051-inch unreinforced series. This again seems to indicate that the addition of rings does not change the creep properties of the basic shell.

Effect of sheet thickness.- Table 3 shows that unreinforced cylinders with sheets of the same material but of different thicknesses have widely varying values of n . There are several possible explanations for this difference; for example, the assumption that equation (6) can adequately describe the creep behavior may not be valid. Other reasons may lie in the differences between the batches from which the sheets were manufactured, in the manufacturing processes the sheets underwent before delivery to the laboratory, and in the amount of coldwork to which they were subjected in the laboratory when cylindrical shells were made from the flat sheet. Certainly the forming operation was more severe for the 0.064-inch sheet than for the 0.032-inch sheet when both were rolled into cylinders of the same radius.

The values of n in table 3 for the reinforced and the 0.051-inch unreinforced cylinders are, with one exception, all between 5.0 and 5.3. This exception, the value 5.8, was obtained on the basis of a comparatively few tests and further testing showed that the value 5.0 was more appropriate. Since the reinforced cylinders were made from a 0.051-inch shell, this observation seems to indicate that, within experimental accuracy and for the range of reinforcement areas and the special cross-sectional shape of reinforcement considered, the creep exponent depends only on the sheet thickness and not on the reinforcements.

Change in vertical diameter.- The change in vertical diameter of the middle cross section of the cylinder was measured in order to verify experimentally Hoff's theory for creep buckling (ref. 1), which supposes that the cylinder collapses by flattening. This quantity was measured successfully with a linear differential transformer in three experiments, two on unreinforced and one on reinforced cylinders. These were the specimens in table 2 numbered 24, 25, and 55 and the maximum values of the ratio of flattening (see fig. 13) to radius were 0.002, 0.004, and 0.004, respectively. These values are very much smaller than the values predicted by use of Hoff's theory. This observation, combined with the fact that none of the buckled specimens showed any appreciable amount of flattening, indicates that collapse by flattening is not the mechanism for failure in creep. It is possible, however, that the flattening triggers the collapse in another mode. Perhaps the rigid end fittings on the specimens prevented the cylinder from flattening according to theory or possibly the measurements were not taken at the cross section where the flattening was greatest. As mentioned before, difficulties were encountered in measuring the change in diameter and the reliability of the results is open to question. Finally, because the construction of the oven did not permit visual observation of the specimens during a test, the exact nature of the development of the failures is not known.

Polytechnic Institute of Brooklyn,
Brooklyn, N.Y., October 15, 1958.

APPENDIX

SIMPLIFIED METHOD FOR CALCULATING CREEP-BUCKLING TIME

Simplification of Hoff's Method

The method proposed by Hoff in reference 2 for calculating the creep-buckling time or critical time of cylinders loaded by end moments involves the numerical integration of two simultaneous differential equations. The critical time can be found to any desired degree of accuracy by taking small enough increments of time in the integration; however, this procedure is very time-consuming and for this reason it would be desirable to simplify the process for calculating the creep-buckling time. This section describes such a simplified method for calculating the critical time. The method is applied to predict values of the creep-buckling time of cylinders similar to those used in the experiments; results are compared with those obtained using the numerical integration and with experiments.

The results of the experiments described in the body of the report show that the rate of change of curvature of the cylinder axis is constant during a portion of the time between load application and failure. This can be seen, for instance, in figure 10, where the rotation of the end plane θ is proportional to the curvature. If the applied bending moment is substantially below that which causes immediate failure of the cylinder, the curvature rate is constant during a very large portion of the time between load application and failure. This indicates that it is reasonable to take the curvature rate as being constant as a rational means of simplifying Hoff's equations, at least when the ratio of creep-buckling moment to static-buckling moment is not close to unity. Thus, instead of the curvature rate $\dot{\kappa}$ varying with time, it will be assumed that $\dot{\kappa}$ has a constant value $\dot{\kappa}_{av}$ which is some average of those curvature rates actually attained during the time period from load application to failure. The plots of θ versus time show that the slope of the curve (which is proportional to the curvature rate) at any point is everywhere greater than or equal to the slope of the straight-line portion of the curve. The constant curvature rate in any experiment is then also a minimum curvature rate and one may write for the above-mentioned average curvature rate

$$\dot{\kappa}_{av} = \eta \dot{\kappa}_s \quad (7)$$

where η is a multiplier greater than or equal to 1 and $\dot{\kappa}_s$ is the steady, constant, or minimum curvature rate. For a particular cylinder and a particular moment, $\dot{\kappa}_s$ may be found from the empirical relation

$$\dot{\kappa}_s = (M/\mu')^n \quad (6)$$

Values for n and μ' have been determined in an earlier part of the report for the cylinders which were used as test specimens. The curvature can be expressed as

$$\kappa = \kappa_0 + \dot{\kappa}_{av}t \quad (8)$$

if the curvature rate is constant. In this equation, κ_0 is the curvature due to the elastic deformation of the cylinder as the load is applied.

The equations of Hoff (eqs. (57) and (58) of ref. 2) which are to be simplified are

$$(\dot{\kappa}r)^{1/n} = \frac{(M/h_e r^2 \lambda J_{1n})}{1 - \left(\frac{n+1}{n}\right)(a/r) \left[1 + \frac{1}{n+1}(\kappa/\dot{\kappa})(\dot{a}/a)\right] (J_3/J_{1n})} \quad (9)$$

$$(\dot{a}/r)^{1/p} = (1/3)^{(p+1)/p} (J_3/J_{1n}J_{1p}) (M\kappa/\mu) r^{1/p} \times \left\{ \frac{1 - (1/n)(a/r) \left[1 + (\kappa/\dot{\kappa})(\dot{a}/a)\right] (J_5/J_3)}{1 - \frac{n+1}{n}(a/r) \left[1 + \frac{1}{n+1}(\kappa/\dot{\kappa})(\dot{a}/a)\right] (J_3/J_{1n})} \right\} \quad (10)$$

where r is the cylinder radius, a is the flattening (see fig. 13), h_e is the effective sheet thickness in the axial direction, n and λ are creep constants for the axial deformations, p and μ are creep constants for the circumferential deformations, and J_{1n} , J_{1p} , J_3 , and J_5 are constants dependent upon n and p .

Substitution of $\dot{\kappa}_{av}$ for κ in equation (9) and subsequent manipulations lead to

$$\frac{1}{(a/r)} \left[1 - \frac{M}{\lambda h_e r^2 J_{1n} (\dot{\kappa}_{av} r)^{1/n}} \right] = \frac{n+1}{n} \left(\frac{J_3}{J_{1n}} \right) \left[1 + \frac{1}{n+1} (\kappa/\dot{\kappa}_{av}) (\dot{a}/a) \right] \quad (11)$$

One can set the second term in the brackets on the left-hand side of equation (11) equal to a constant or

$$\frac{M}{\lambda h_e r^2 J_{1n} (\dot{\kappa}_{av} r)^{1/n}} = C \quad (12)$$

Use of equation (12) in equation (11) and further manipulations result in

$$(\kappa/\dot{\kappa}_{av}) (\dot{a}/a) = \frac{J_{1n}}{J_3} \left(\frac{n}{a/r} \right) (1 - C) - (n+1) \quad (13)$$

Comparison of equations (9) and (12) shows that

$$1 - \left(\frac{n+1}{n} \right) (a/r) \left[1 + \frac{1}{n+1} (\kappa/\dot{\kappa}_{av}) (\dot{a}/a) \right] \left(J_3/J_{1n} \right) = C \quad (14)$$

Substitution of $(\kappa/\dot{\kappa}_{av}) (\dot{a}/a)$ from equation (13) into the numerator of equation (10) and introduction of equation (14) into the denominator of equation (10) results in

$$\left(\frac{\dot{a}}{r} \right)^{1/p} = \left(\frac{1}{J_3} \right)^{\frac{p+1}{p}} \left(\frac{J_3}{J_{1n} J_{1p}} \right) \left(\frac{M \kappa}{\mu} \right) r^{1/p} \left[\frac{1 + \frac{a}{r} \frac{J_5}{J_3} - \frac{J_{1n}}{J_3} \frac{J_5}{J_3} (C - 1)}{C} \right] \quad (15)$$

Equation (15) is of the form

$$(\dot{\alpha}/\dot{t})^{1/p} = C_1 \kappa (C_2 + \alpha) \quad (16)$$

where

$$C_1 = (1/3)^{\frac{p+1}{p}} \left(\frac{J_3}{J_{1n} J_{1p}} \right) \left(\frac{1}{C} \right) \left(\frac{J_5}{J_3} \right) \left(\frac{M r^{1/p}}{\mu} \right)$$

$$C_2 = \left(J_3/J_5 \right) \left[1 + \frac{J_{1n} J_5}{J_3^2} (1 - C) \right]$$

$$\alpha = a/r$$

Use of the value of κ from equation (8) in equation (16) results in

$$d\bar{\alpha}/(1 + \bar{\alpha})^p = C_2^{p-1} C_1^p (1 + \bar{t})^p \left(\kappa_0^{p+1} / \dot{\kappa}_{av} \right) d\bar{t} \quad (17)$$

where

$$\bar{\alpha} = \alpha/C_2$$

$$\bar{t} = \dot{\kappa}_{av} t / \kappa_0$$

The region of integration for equation (17) is to extend over the period from load application to failure. Then $\bar{\alpha}$ is to be integrated between the limits $\bar{\alpha}_0$ and $\bar{\alpha}_{cr}$ where $\bar{\alpha}_0$ is the nondimensionalized initial or elastic flattening and $\bar{\alpha}_{cr}$ is the nondimensionalized flattening at which the cylinder, for all practical purposes, has failed. The latter value will be obtained from the criterion for failure used in reference 2, $(a/r)_{cr} = 0.20$. The limits of integration on \bar{t} will be from zero to \bar{t}_{cr} , the nondimensionalized time parameter corresponding to failure.

Upon integration equation (17) becomes

$$\left(\frac{p+1}{1-p}\right) \frac{\dot{\kappa}_{av}}{\kappa_0^{p+1} C_1^p C_2^{p-1}} \left[\frac{1}{(1+\bar{\alpha}_{cr})^{p-1}} - \frac{1}{(1+\bar{\alpha}_0)^{p-1}} \right] + 1 = (1+\bar{t}_{cr})^{p+1} \quad (18)$$

or

$$\bar{t}_{cr} = \left\{ \left(\frac{p+1}{1-p}\right) \frac{\dot{\kappa}_{av}}{\kappa_0^{p+1} C_1^p C_2^{p-1}} \left[\frac{1}{(1+\bar{\alpha}_{cr})^{p-1}} - \frac{1}{(1+\bar{\alpha}_0)^{p-1}} \right] + 1 \right\}^{1/(p+1)} - 1 \quad (19)$$

When the ratio of moment to static-buckling moment is much less than 1, the experiments showed that the average value of the curvature is not much greater than the constant value. Then for an applied bending moment much less than the static-buckling moment, one may use the approximation that $\eta = 1$ and equation (7) becomes

$$\dot{\kappa}_{av} = \dot{\kappa}_s \quad (20)$$

where $\dot{\kappa}_s$ is obtained from equation (6). Now if the equilibrium of a cross section of the cylinder is considered, there results

$$M = 4 \int_0^{\pi/2} \sigma r^2 h_e \cos \psi \, d\psi \quad (21)$$

The creep law of the material is given by

$$\sigma = \dot{\epsilon}^{1/n_\lambda} \quad (22)$$

The condition that plane sections of the cylinder remain plane during bending is

$$\epsilon = \kappa r \cos \psi \quad (23)$$

Insertion of the value of ϵ from equation (23) into equation (22), use of the resulting expression in equation (21), and some manipulations result in

$$\lambda = \frac{M}{J_{1n} h e r^2 (r \kappa_s)^{1/n}} \quad (24)$$

Use of equation (20) in equation (24) and comparison with equation (12) shows that $C = 1$ when one assumes $\eta = 1$. The equations for C_1 and C_2 then reduce to

$$C_1 = (1/3)^{(p+1)/p} \left(J_5 / J_1^2 \right) (M/\mu) r^{1/p} \quad (25)$$

$$C_2 = J_3 / J_5 \quad (26)$$

Because of equations (6), (25), and (26), equation (17) can be written as

$$\begin{aligned} (1 + \bar{t}_{cr})^{p+1} = & \left[\left(\frac{p+1}{1-p} \right) \left(\frac{J_3}{r J_5} \right) \left(\frac{J_{1n} J_{1p}}{J_3} \right)^p \left(\frac{3}{\kappa_0} \right)^{p+1} M^{n-p} \frac{\mu^p}{(\mu')^n} \right] \times \\ & \left[\left(\frac{1}{1 + \bar{\alpha}_{cr}} \right)^{p-1} - \left(\frac{1}{1 + \bar{\alpha}_0} \right)^{p-1} \right] + 1 \end{aligned} \quad (27)$$

Equation (27) may be used to calculate the creep-buckling time of reinforced cylinders. The equation can be simplified for the case of unreinforced cylinders. In this case $n = p$, $h = h_e = h_p$, and the relation between μ and λ is

$$\mu = (1/2)^{(2n+1)/n} \left[2n/(2n+1) \right] \lambda h^{(2n+1)/n} \quad (28)$$

If equation (6) is considered, equation (24) can be written as

$$\mu' = J_{1n} h_e \lambda r^{(2n+1)/n} \quad (29)$$

Use of equations (28) and (29) in equation (27) results in

$$\bar{t}_{cr} = \left\{ \frac{F_1}{(r^2 \kappa_0)^{n+1}} \left[\frac{1}{(1 + \bar{\alpha}_{cr})^{n-1}} - \frac{1}{(1 + \bar{\alpha}_0)^{n-1}} \right] + 1 \right\}^{1/(n+1)} - 1 \quad (30)$$

where

$$F_1 = \left(\frac{n+1}{1-n} \right) (3)^{n+1} \left(\frac{J_3}{J_5} \right) \left[\frac{2J_{1n}}{J_3 h (2n+1)} \right]^n (h/2)^{2n+1}$$

In all the numerical examples subsequently worked with this method, it was assumed that $\eta = 1$ so that equations (27) and (30) could be used for calculating the critical times of reinforced and unreinforced cylinders, respectively.

Calculation of the critical time is then carried out in the following manner:

- (1) The creep constants n , p , μ , and μ' are obtained from experiments and the quantities J_3 , J_5 , J_{1n} , and J_{1p} are calculated
- (2) From an elastic or an elastoplastic analysis, κ_0 and $\bar{\alpha}_0 = (1/C_2)(a/r)$ are obtained (the next section discusses this calculation)
- (3) Equation (27) or (30) is used to determine \bar{t}_{cr}
- (4) Finally, with $\dot{\kappa}_{av}$ from equation (6), the critical time is obtained from $\bar{t} = \dot{\kappa}_{av}t/\kappa_0$

This simplification of Hoff's method was used to calculate the creep-buckling times of the cylinders used in the experiments. Enough examples were calculated so that it was possible to draw curves of bending moment against critical time for each type of cylinder tested. These curves are shown in figure 14.

Elastic Flattening and Elastic Curvature

The initial or elastic values of the flattening and curvature are needed to calculate the critical time if one uses either the method of reference 2 or the simplification of this method developed in the previous section. These elastic quantities can be found directly from the following equations derived by Hoff in reference 2:

$$\kappa = \frac{M}{E\pi r^3 h_e \left[1 - (3/2)(a/r) \right]} \quad (31)$$

and

$$M = E\pi r^3 h_e \kappa \left[1 - \frac{(3/2)T(r\kappa)^2}{1 + (5/6)T(r\kappa)^2} \right] \quad (32)$$

where $T = (h_e/h_b)(r/h_b)^2$ and h_b is the effective thickness of sheet that resists circumferential deformations. The calculations, however, involve the solution of a cubic equation (eq. (32)) and present practical difficulties. A perturbation method will now be derived to simplify the calculation of the elastic deformations.

The assumption is made that the elastic curvature κ_0 may be written as:

$$\kappa_0 = \kappa_1(1 + e) \quad (33)$$

where $\kappa_1 = M/EI$ and e is a small number representing the correction to simple beam theory which is necessary in the case of a thin-walled cross section. Substitution of κ_0 from equation (33) into equation (32) and neglect of powers of e higher than the second lead to the quadratic

$$e^2 + (2/17) \left(\frac{11\kappa_1^2 Tr^2 - 3}{\kappa_1^2 Tr^2} \right) e + (9/17) = 0 \quad (34)$$

Manipulation of equation (31) and consideration of equation (33) results in an expression for the elastic flattening ratio $(a/r)_0$ which is

$$(a/r)_0 = (2/3) [e/(1 + e)] \quad (35)$$

The elastic curvature and flattening ratio can then be obtained by first solving equation (34) for e and then using this value of e in equations (32) and (35) to compute κ_0 and $(a/r)_0$. This procedure was used to calculate the elastic quantities for the integrations described in the previous section.

The accuracy of both the above method and Hoff's method for calculating elastic flattening and curvature was investigated by means of numerical examples. Results obtained using these approximate methods were compared with the results obtained by an exact solution of equations (31) and (32). Unreinforced cylinders of 0.040-inch thickness and loaded by end moments in the range from 30,200 to 51,800 inch-pounds were used in the numerical examples. In this range of loads it was

found that the values of the elastic curvature as calculated by the three methods were all within 1 percent of one another. However, the values of the elastic flattening ratio as calculated by the perturbation method were found to be lower and the values as calculated by Hoff's method were found to be higher than the exact values. For a moment of 51,800 inch-pounds, the former method gave a value 7 percent too high, while the latter gave a value 5 percent too low; the differences were less for lower loads.

The results of the examples using both the numerical integration and the simplified integration to calculate the critical time show that the values of flattening and curvature at failure are of the order of 10 times the elastic values. For creep-buckling problems, then, it is probably immaterial which of the three methods discussed is used to calculate the elastic flattening and curvature because a small error in initial values will not affect the critical time very much.

If it is desired to obtain a plot of moment versus flattening for an elastic-buckling problem, equations (31) and (32) should probably be used to calculate the flattening. The reason for using the exact solution is that the approximate methods seem to yield values for the flattening that diverge from the exact values as the load approaches the buckling load.

Effect of Plastic Deformations on Critical Time

A possible reason for the discrepancy between theoretical and experimental values of the critical time at high loads is that the material in some parts of the cylinder has exceeded the proportional limit, with the consequence that Young's modulus no longer defines the stress-strain relation. If this is true, Young's modulus must be replaced by a reduced modulus in the calculation of the critical time. The resulting decrease in bending rigidity will cause larger initial deformations and thus hasten the onset of buckling.

As an example, the case of a 0.040-inch cylinder loaded with a 54,400-inch-pound moment (test 24) was considered. The experimental critical time for this cylinder was 3 minutes while the simplified theory predicted a critical time of 29 minutes. Using the M_y/I relation it would be found that $\sigma_{\max} = (\sigma)_{y=r} = 6,770$ psi. A stress-strain curve for the material at the temperature of the test, as obtained in a private communication from Mr. E. C. Hartmann of the Aluminum Co. of America, shows that the proportional limit is about 3,000 psi, so that a calculation of the reduced modulus is necessary.

It will be assumed that plane sections of the cylinder before bending remain plane after bending, so that

$$\epsilon = y/\rho \quad (36)$$

where y is the distance from the neutral axis, ρ is the radius of curvature of the neutral axis, and ϵ is the axial strain. Because of this proportionality between ϵ and y , the stress distribution at a section has the same shape as part of the stress-strain curve. Thus if the stress $(\sigma)_{y=r}$ on the extreme fiber is known, the stress distribution of figure 15(a) is determined from the stress-strain curve of the material (fig. 16). The stress $(\sigma)_{y=r}$ will be determined by the consideration that the moment of the stresses at a section must equal the applied moment. This can be written as

$$M = (4h)\Sigma\sigma y r \Delta\psi \quad (37)$$

where the summation is taken over the section shown in figure 15(b).

The correct stress distribution is then found by a trial-and-error procedure as follows:

- (1) Assume a value of $(\sigma)_{y=r}$ in figure 16. This determines the distribution of σ in figure 15(a).
- (2) Calculate M from equation (37). If this value does not agree with the original moment, choose another $(\sigma)_{y=r}$ and recalculate M until it is in agreement with the original value.

This procedure was carried out for the example mentioned above and it was found that $(\sigma)_{y=r} = 6,100$ psi. The strain corresponding to this stress from figure 16 is $(\epsilon)_{y=r} = 0.00122$ inch per inch. With this value of ϵ and with $y = r$, one obtains from equation (36) $\rho = 6,560$ inches. From the equation

$$E_r = M\rho/I \quad (38)$$

a value was obtained for

$$E_r = 5.6 \times 10^6 \text{ psi}$$

as compared with the value $E = 8 \times 10^6 \text{ psi}$ used in the calculations.

This value of E_r can be used for calculating the initial deflections and the critical time. When this was done it was found that

- (1) The initial flattening ratio $(a/r)_0$ was increased by a factor of 2.1.
- (2) The initial curvature κ_0 was increased by a factor of 1.7.
- (3) The critical time t_{cr} was decreased from 29 minutes to 24 minutes.

Thus it appears that the inclusion of initial inelastic behavior in the theory cannot alone explain the discrepancies between theory and experiment for critical time at high loads.

Discussion

In figure 14, the values of the critical time obtained from the experiments are compared with the values predicted by use of Hoff's theory and by use of the simplified version of this theory. The agreement between the results from the two theories is seen to be close for all types of specimens compared.

The agreement between the results of theory and experiment for the unreinforced specimens is good at comparatively low values of the load but poor at high values of the load. For the ring-reinforced specimens, the agreement is seen to be very poor. The critical times were calculated only for the type I series since the necessary creep data were not available for the type H series, but it is felt that a similar result would have been obtained for the latter. It should be noted, however, that, in the case of the ring-reinforced specimens, the failures were due to local instability although the theory is based upon the assumption of a general instability. The longitudinally reinforced cylinders give reasonably good agreement between theory and experiment throughout the entire range of loads. For the longitudinally and circumferentially reinforced cylinders, the agreement is excellent for the type F and very poor for the type J specimens. This difference in behavior probably arises from the fact that the former had rings of greater flexibility than the latter.

This behavior plus the poor agreement in the case of just ring reinforcements leads one to the conclusion that the theory overestimates the increase in buckling strength due to the presence of rings.

In general, applications of the theory give values for the critical time that are unconservative. The shape of the curve of moment versus critical time is such that the prediction of the critical time for a given moment can be in great error for comparatively low values of the moment. The prediction of the moment that will cause failure in a given time, however, will probably result in a smaller error. Use of the theoretical curve in the range near the instantaneous buckling load is not recommended as the experiments have shown a large amount of scatter in this region.

The values of $n = 5.8$ and $\mu' = 431,000$ were used to calculate the critical times for the 0.051-inch unreinforced cylinders instead of the values $n = 5.0$ and $\mu' = 577,000$ which were later determined to be more appropriate when the 30-inch-cylinder test points were considered. The latter values were used in one example to determine how the critical time would be changed if these values were used in the calculations. It was found that for cylinder 20 the critical time, as calculated by the numerical integration, was reduced from 205 to 175 minutes. The experimental value of the critical time for this cylinder was 130 minutes so that the use of $n = 5.0$ and $\mu' = 577,000$ should increase the agreement between theory and experiment for this type of specimen. This also illustrates the need for an accurate determination of the creep constants from the experimental data in order to predict the creep-buckling time.

In the calculations of the critical times for the various types of specimens, it was found that the use of the simplified method enabled one to obtain a curve of moment versus critical time in approximately one-quarter of the time needed to obtain a similar curve by use of the numerical integration. Since figure 14 shows that the results obtained by the two methods are almost identical, the use of the simplified method seems justified in calculating the critical time.

It is instructive to compare the variation of curvature with time during a test as obtained from use of the two theories and from the experimental measurements. The comparison is made for a test (test 31) in which the predicted and experimental values of critical time were almost identical (see table 2 and fig. 14(a)). The curves are shown in figure 17, and it is seen that the agreement between all three curves is very good for the majority of the test period. The curves show that, in this case at least, the assumption made in the simplified theory as to the constancy of the curvature rate is valid and leads to excellent results in predicting the critical time.

The criterion for failure was that when the flattening ratio reached a value of 0.20 the cylinder was considered to have failed. This criterion was used by Hoff in reference 2 and perhaps was chosen on the basis of the result of Brazier's work on elastic buckling, which showed that a cylinder became unstable when the flattening ratio attained a value of $2/9$ or 0.22. The effect of the somewhat arbitrary choice of the critical flattening ratio on the critical time was investigated by means of an example. Critical times for the cylinder of test 38 were calculated by using critical flattening ratios of 0.10, 0.20, and ∞ in the simplified integration. The results of this example are summarized below; for comparison, the corresponding experimental value was 92 minutes.

α_{cr}	$t_{cr}, \text{ min}$
0.10	73
.20	88
∞	118

REFERENCES

1. Erickson, Burton, Patel, Sharad A., French, Frances W., Lederman, Samuel, and Hoff, N. J.: Experimental Investigation of Creep Bending and Buckling of Thin Circular Cylindrical Shells. NACA RM 57E17, 1957.
2. Hoff, N. J.: Buckling at High Temperature. Jour. R.A.S., vol. 61, no. 563, Nov. 1957, pp. 756-774.
3. French, Frances W., and Erickson, Burton: Further Creep Buckling Tests With Cylinders Subjected to Flexure. PIBAL Rep. No. 412, Polytechnic Inst. of Brooklyn, July 1957.

W
1
4
1

TABLE 1.- SUMMARY OF TESTS

[All sheets and stiffeners were manufactured of 5052-0 aluminum alloy unless otherwise specified]

Specimen code letter	Sheet thickness, in.	Cylinder			Number of tests			
		Length, in.	Reinforcement		Creep	Static		Total
			Longitudinal, number (a)	Circular, number		500° F	Room temperature	
None	0.064	40	---	---	12	1	1	14
None	.051	40	---	---	5	1	1	7
None	.040	40	---	---	8	3	---	11
None	.032	40	---	---	7	4	1	12
A	.051	30	---	---	8	2	---	10
B	.032	40	16	---	2	---	1	3
C	.051	40	16	---	5	1	---	6
D	.051	40	16	a ₇	1	---	---	1
E	.051	40	16	b ₇	1	---	---	1
F	.051	40	16	b c ₇	7	1	---	8
G	.051	40	12	---	6	1	1	8
H	.051	40	---	a ₇	4	1	2	7
I	.051	40	---	a ₁₉	6	1	1	8
J	.051	40	12	a ₇	5	1	---	6

^aStiffener cross section of 1/4 by 1/2 inch.

^bStiffener cross section of 1/8 by 1/2 inch.

^cCircular stiffener manufactured of 2024-T4 aluminum alloy.

TABLE 2.- CRITICAL TIMES

Cylinder	Thickness, in.	Temperature, °F	Bending moment, in-lb	Time to failure, min
1	0.064	Room	186,400	Static
2	.064	500	115,000	Static
3	.064	500	114,600	0.4
4	.064	500	100,000	12.5
5	.064	500	90,100	26.5
6	.064	500	80,000	39.1
7	.064	500	75,000	64
8	.064	500	70,000	105
9	.064	500	65,200	109
10	.064	500	65,000	130
11	.064	500	63,500	166
12	.064	500	62,000	249
13	.064	500	60,500	233
14	.064	500	55,100	321
15	.051	500	114,100	Static
16	.051	500	86,800	1.0
17	.051	500	62,700	14
18	.051	500	59,400	52
19	.051	500	54,000	86
20	.051	500	48,600	130
21	.040	500	75,200	Static
22	.040	500	84,500	Static
23	.040	500	70,600	Static
24	.040	500	54,400	3
25	.040	500	51,800	11
26	.040	500	49,100	37
27	.040	500	44,800	29
28	.040	500	44,800	40
29	.040	500	41,000	75
30	.040	500	34,600	178
31	.040	500	30,200	370
32	.032	Room	52,100	Static
33	.032	500	43,700	Static
34	.032	500	48,600	Static
35	.032	500	52,300	Static
36	.032	500	37,800	7
37	.032	500	32,400	69
38	.032	500	29,600	92
39	.032	500	27,000	116
40	.032	500	24,600	269
41	.032	500	21,600	288
42	.032	500	20,500	449
43	.032	500	46,200	Static
44	.051	500	119,500	Static
45	.051	500	119,100	Static
46	.051	500	96,300	2.7
47	.051	500	75,200	19.2
48	.051	500	75,200	24.8
49	.051	500	62,600	33.5
50	.051	500	52,900	44.5
51	.051	500	50,400	145.0

TABLE 2.- CRITICAL TIMES - Concluded

Cylinder	Thickness, in.	Temperature, °F	Bending moment, in-lb	Time to failure, min
52	0.051	500	43,200	105
53	.051	500	37,000	717.8
54	.032	Room	93,700	Static
55	.032	500	51,600	11.2
56	.032	500	46,200	28.2
57	.051	500	189,600	Static
58	.051	500	113,500	18.3
59	.051	500	93,900	57.4
60	.051	500	88,700	118.7
61	.051	500	84,800	140
62	.051	500	72,100	209
63	.051	500	113,500	77
64	.051	500	113,500	44.5
65	.051	500	176,500	Static
66	.051	500	170,000	5.2
67	.051	500	129,600	27
68	.051	500	118,800	55
69	.051	500	108,000	95
70	.051	500	102,600	100
71	.051	500	99,900	159
72	.051	500	95,000	155
73	.051	Room	209,400	Static
74	.051	Room	117,500	Static
75	.051	Room	120,200	Static
76	.051	500	108,400	Static
77	.051	500	181,000	Static
78	.051	500	46,000	166
79	.051	Room	109,500	Static
80	.051	500	43,000	329
81	.051	500	55,000	77
82	.051	500	100,000	32
83	.051	500	70,000	21.5
84	.051	500	70,100	152
85	.051	500	80,000	74.5
86	.051	500	67,500	131
87	.051	500	67,500	156.5
88	.051	Room	123,700	Static
89	.051	500	80,000	6.8
90	.051	500	49,000	115
91	.051	500	45,000	318.5
92	.051	500	47,000	142
93	.051	500	50,000	128
^a 94	.051	500	46,000	
95	.051	500	112,400	Static
96	.051	500	174,700	Static
97	.051	500	62,700	402
98	.051	500	127,000	8
99	.051	500	100,000	60
100	.051	500	80,000	123
101	.051	500	80,000	296
102	.051	500	90,000	95.5

^aSpecimen was of 5052-H34 aluminum alloy; test terminated after 380 minutes without failure.

TABLE 3.- CREEP CONSTANTS

Specimen code letter or sheet thickness, in.	n	μ' , $\text{lb}(\text{in.} \cdot (\text{n}+1)/\text{n})(\text{min}^{\text{L}}/\text{n})$	λ , $\frac{\text{min}^{\text{L}}/\text{n}_{\text{lb}}}{\text{sq in.}}$	μ , $\frac{\text{min}^{\text{L}}/\text{n}_{\text{in.}} \cdot \text{L}/\text{n}_{\text{lb}}}{\text{min}^{\text{L}}/\text{n}_{\text{in.}} \cdot \text{L}/\text{n}_{\text{lb}}}$	p
0.032	3.5	1,080,000	79,000	5.45	3.5
0.040	4.1	796,000	51,000	6.93	4.1
0.051 (based on 40-in. points)	5.8	431,000	23,800	7.60	5.8
0.051 (based on both 30- and 40-in. points)	5.0	577,000	30,900	8.77	5.0
C	5.2	815,500	24,800	8.77	5.0
F	5.3	880,000	26,900	24.6	5.6
G	5.2	734,000	25,200	8.77	5.0
I	5.0	577,000	31,700	320	5.9
J	5.1	840,000	28,300	133	5.9

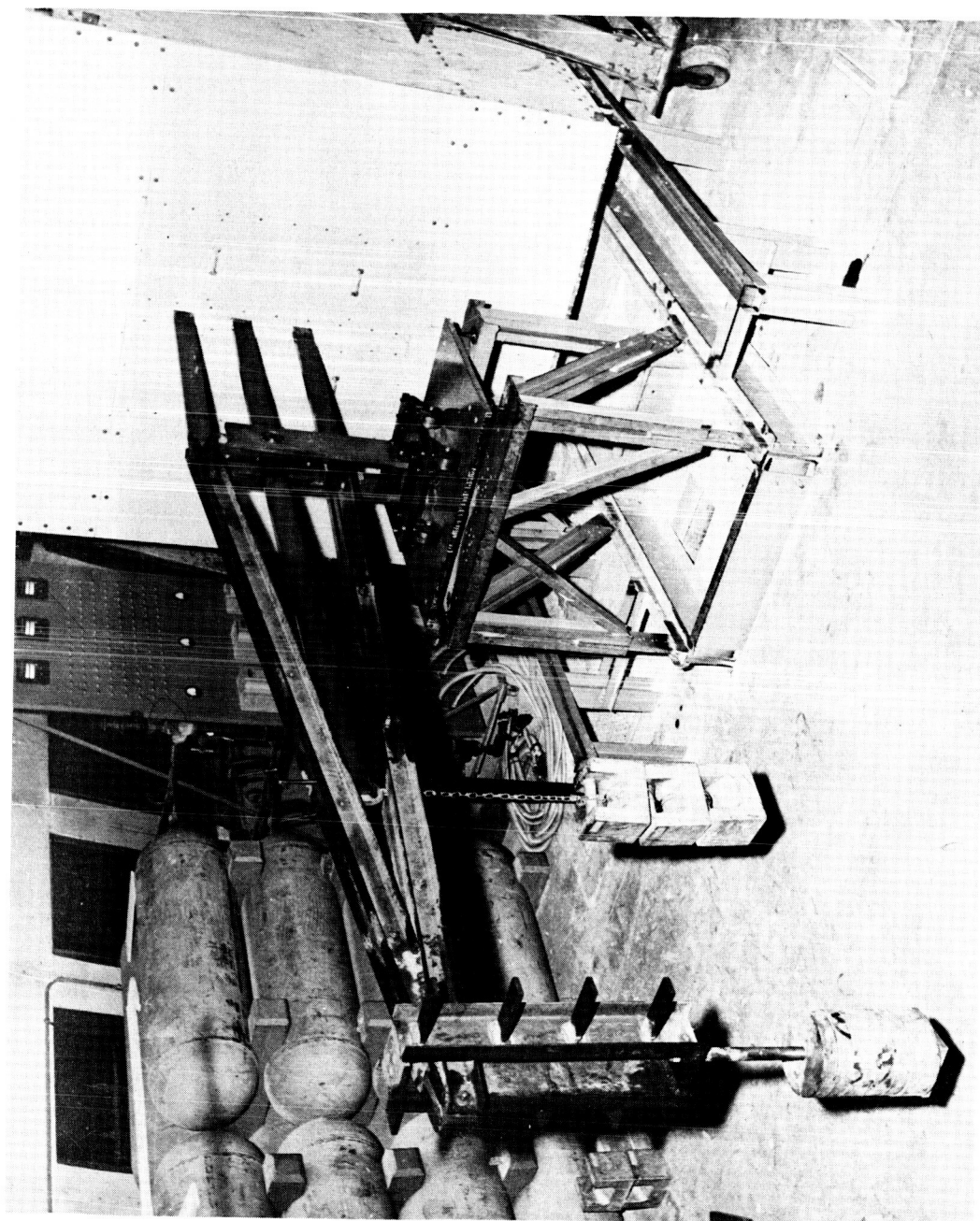
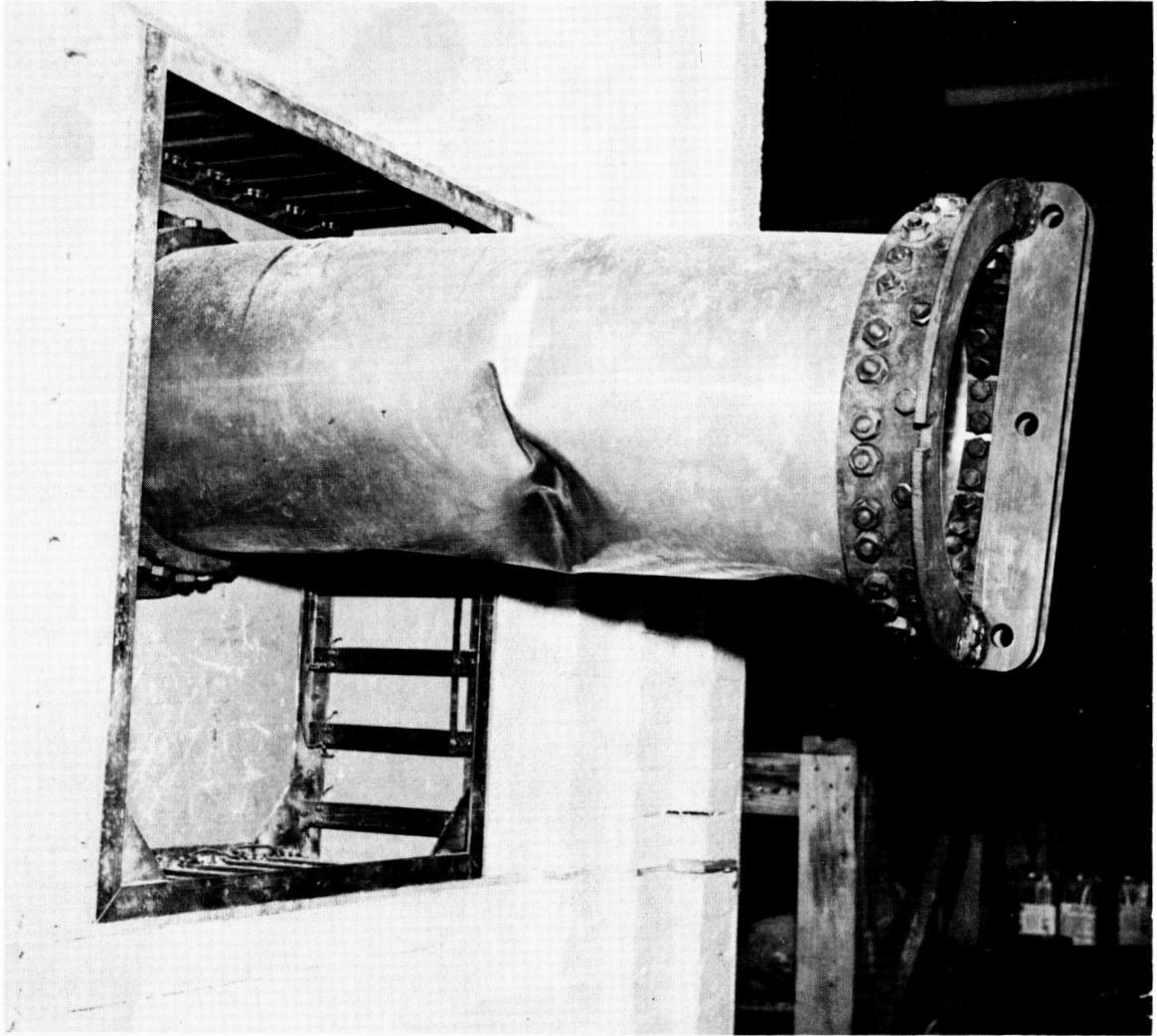


Figure 1.- Loading lever and counterweight. L-57-2546



L-57-2547
Figure 2.- Specimen after failure showing attachment to loading ring.

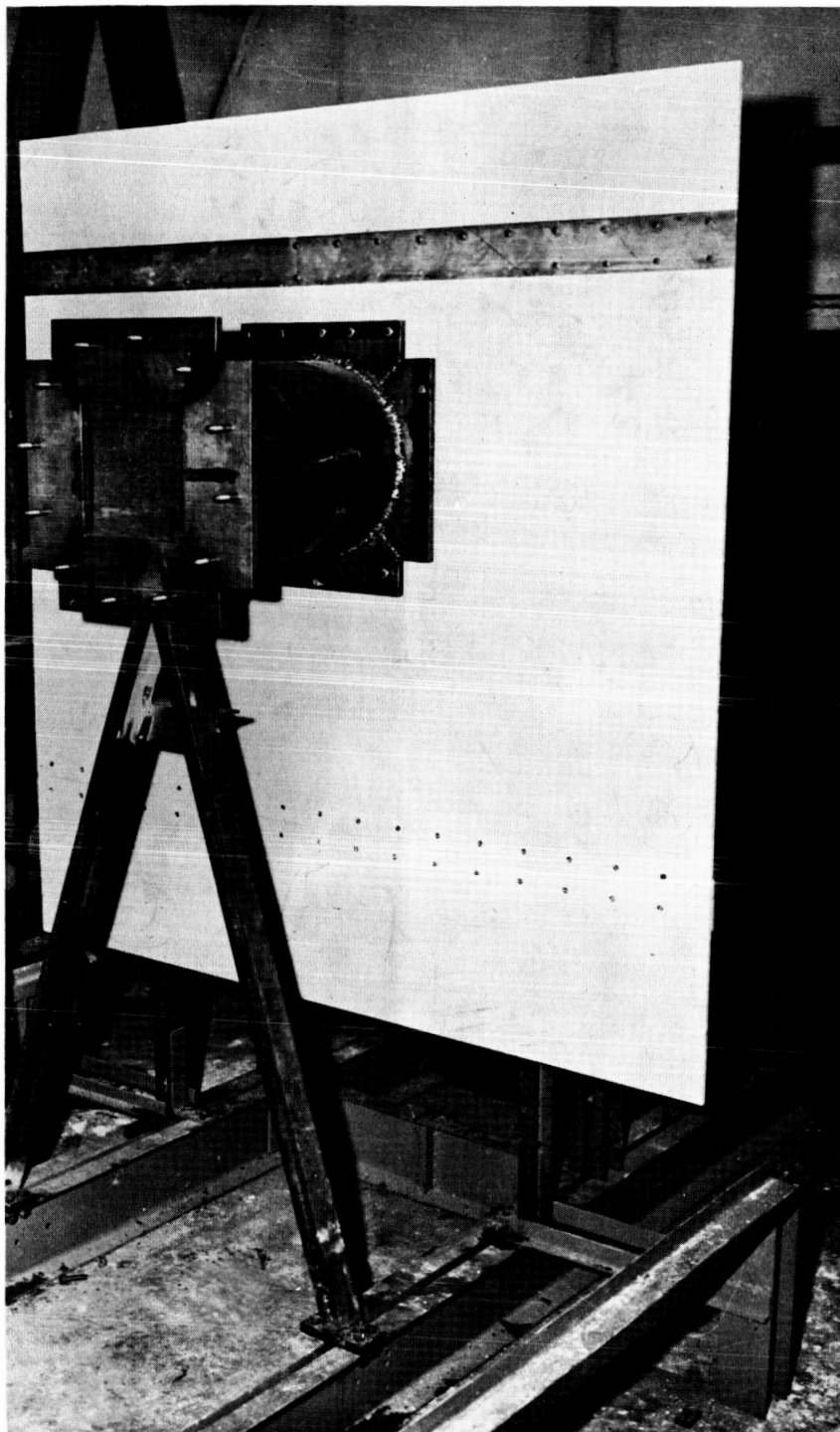


Figure 3.- Strongback attachment cylinder. L-57-2548

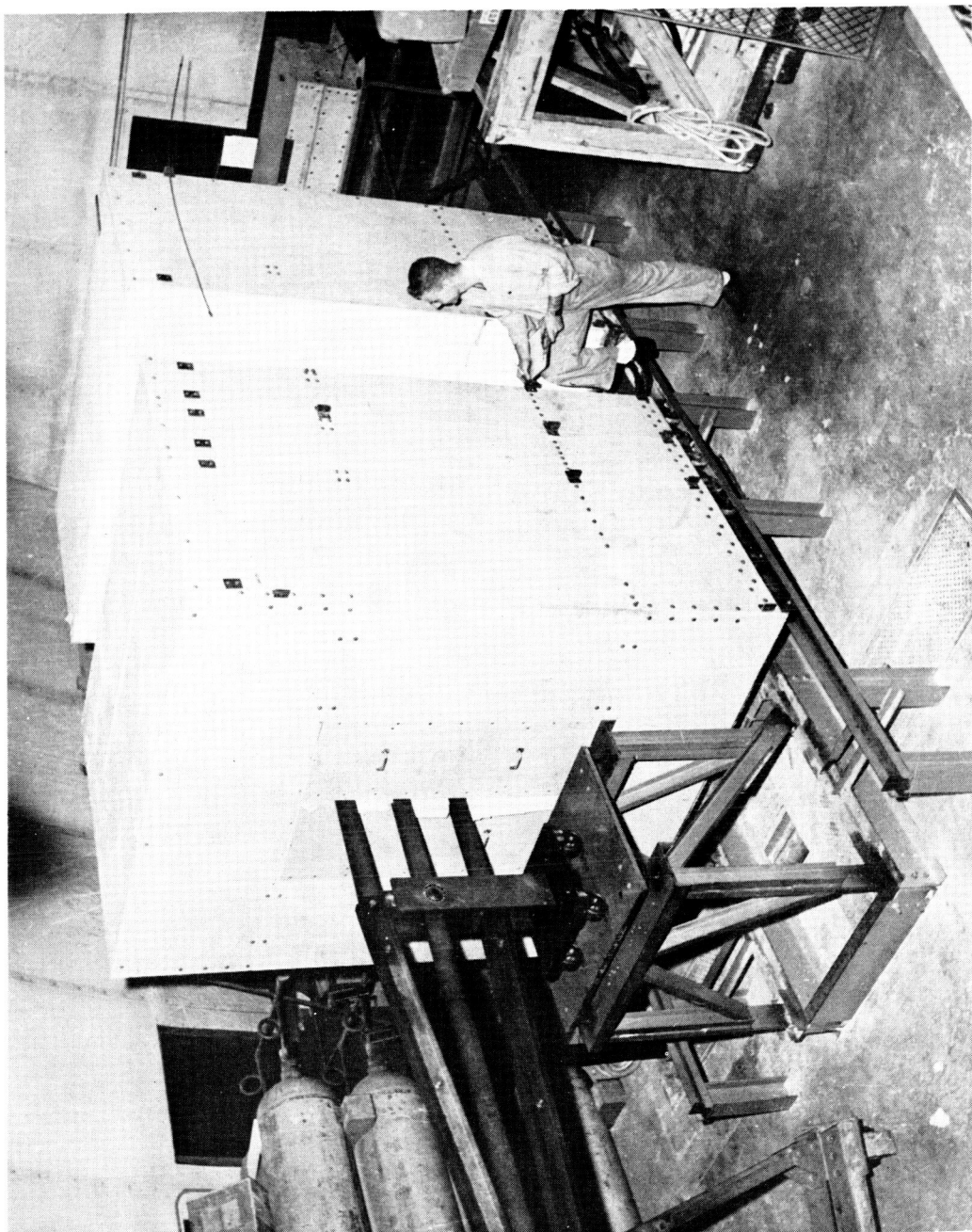
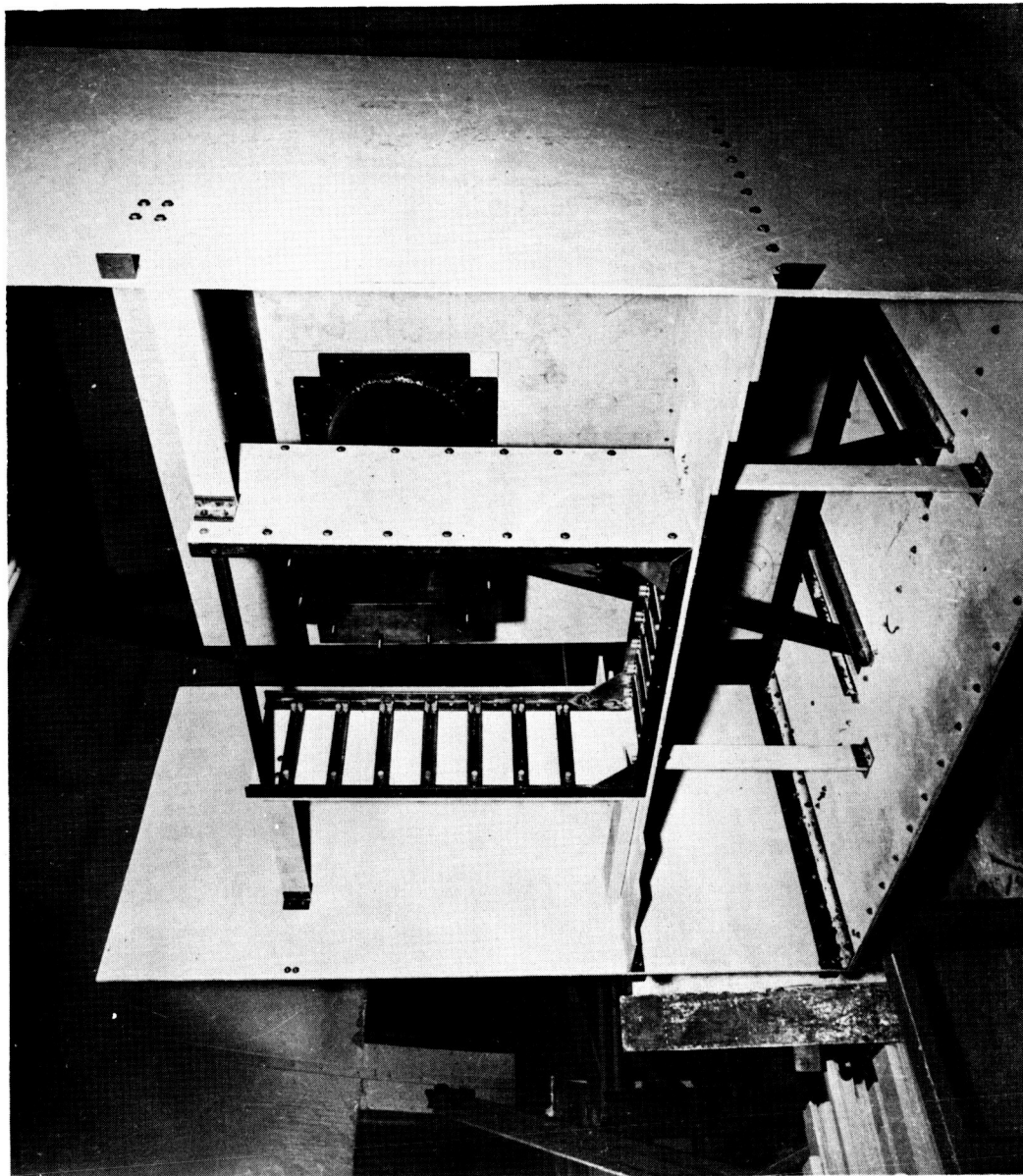


Figure 4.- Overall view of oven. L-57-2549



Figure 5.- Partially completed section of oven. L-57-2550



L-57-2551
Figure 6.- Skeleton of an oven section before installation of insulation.

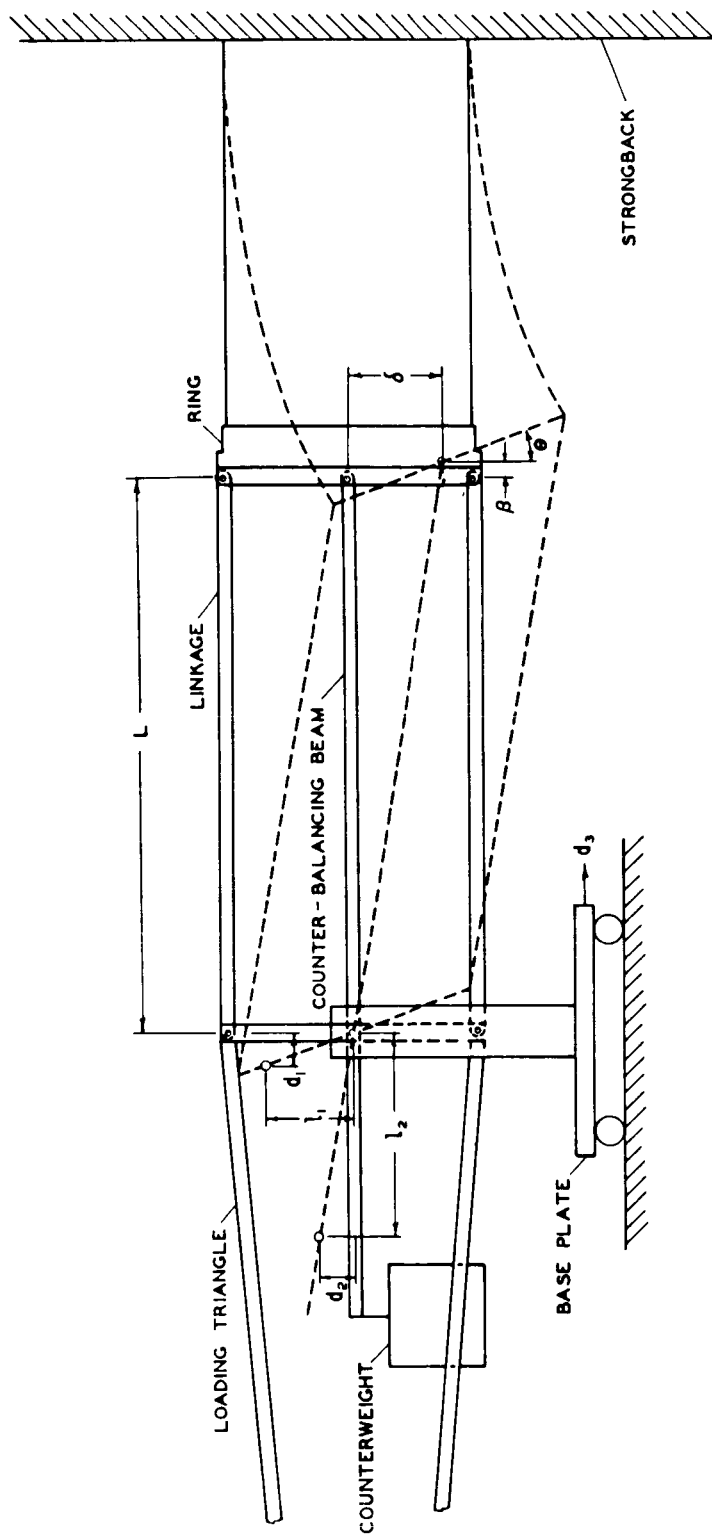


Figure 7.- Schematic drawing of equipment to measure deflections.

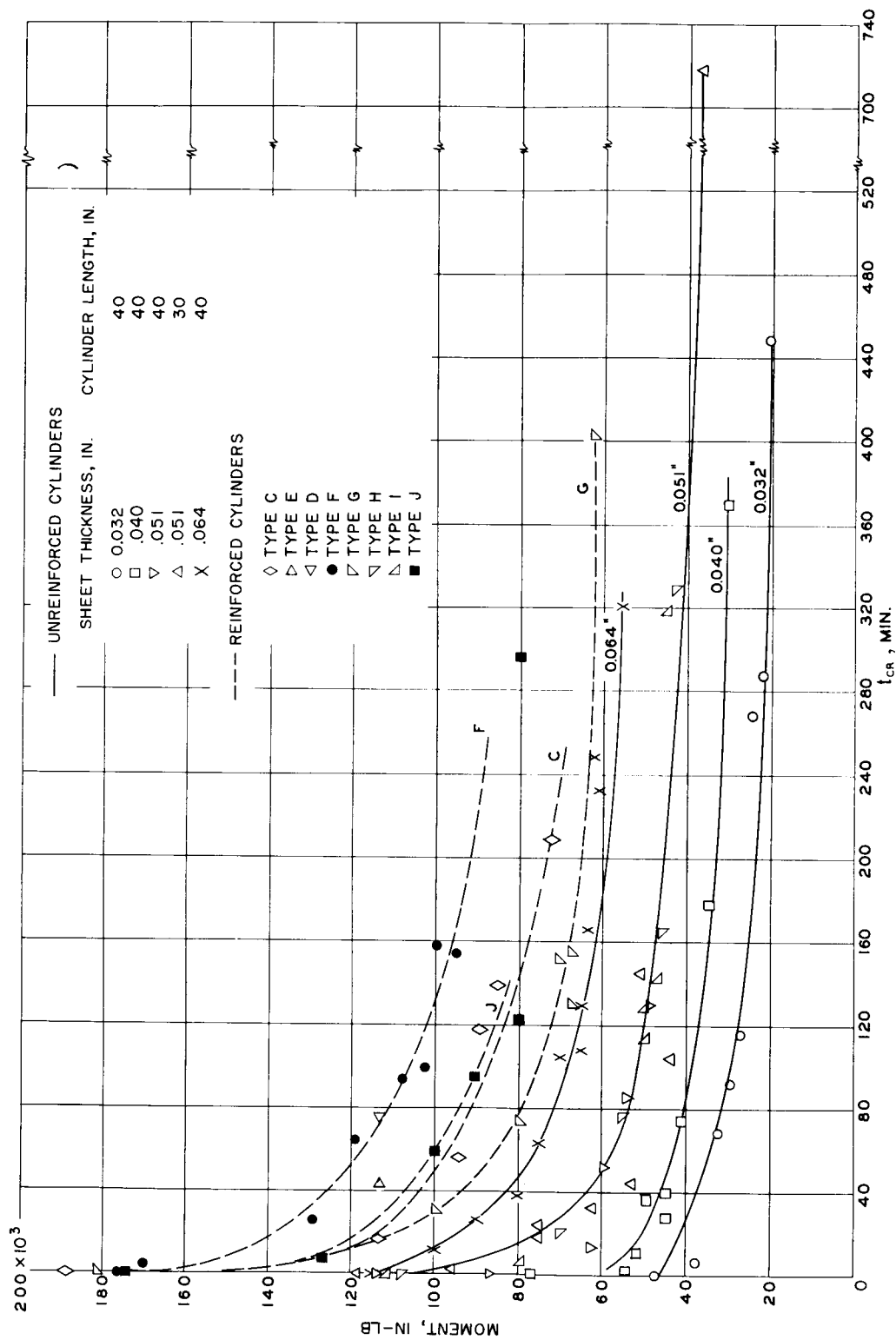
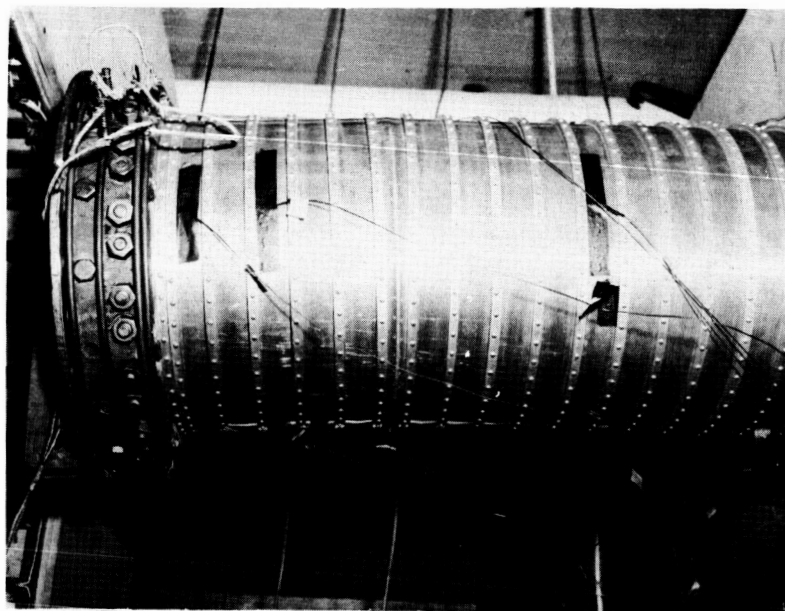
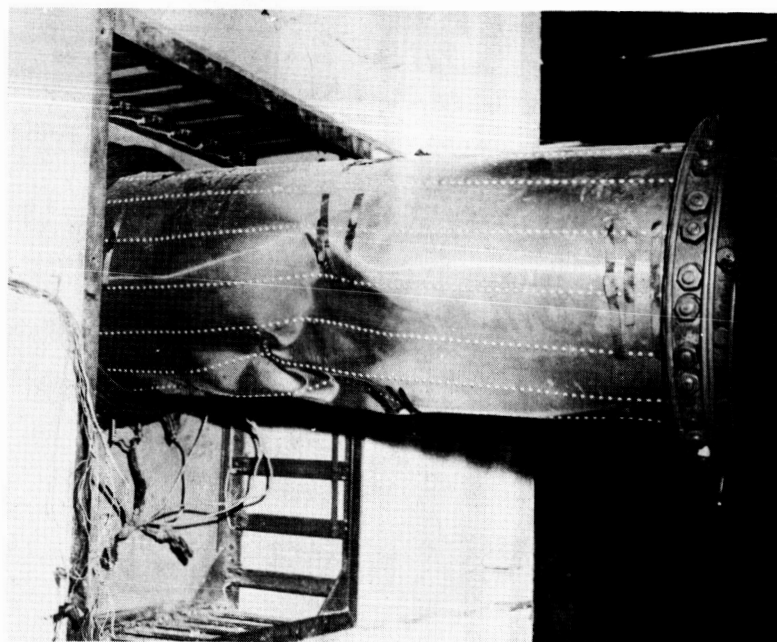


Figure 8.- Moment versus critical time (experimental).



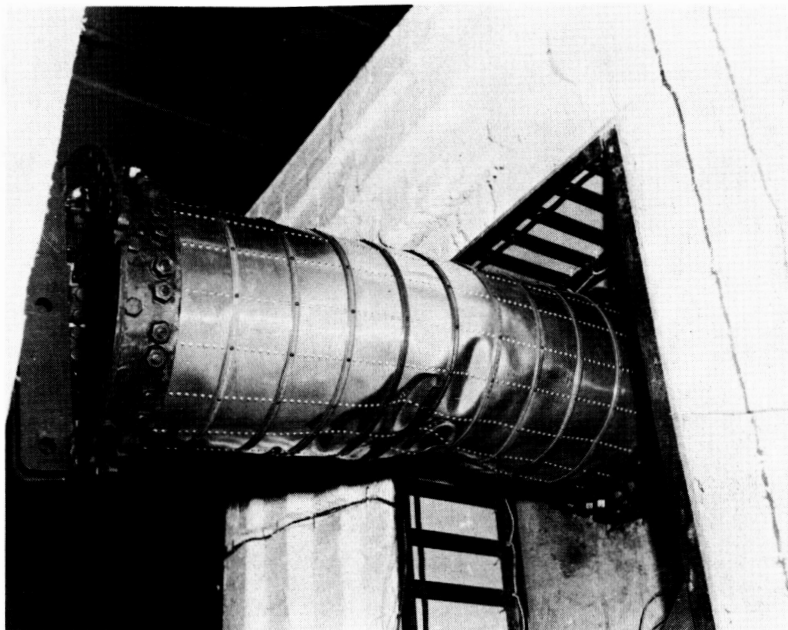
(a) Type I, experiment 92.



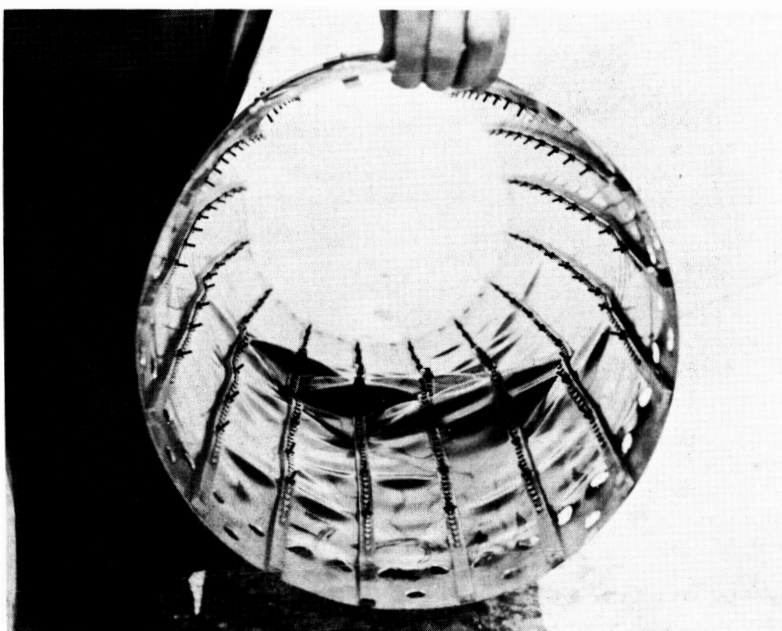
(b) Type C, experiment 58.

L-60-276

Figure 9.- Photographs of specimens after failure.



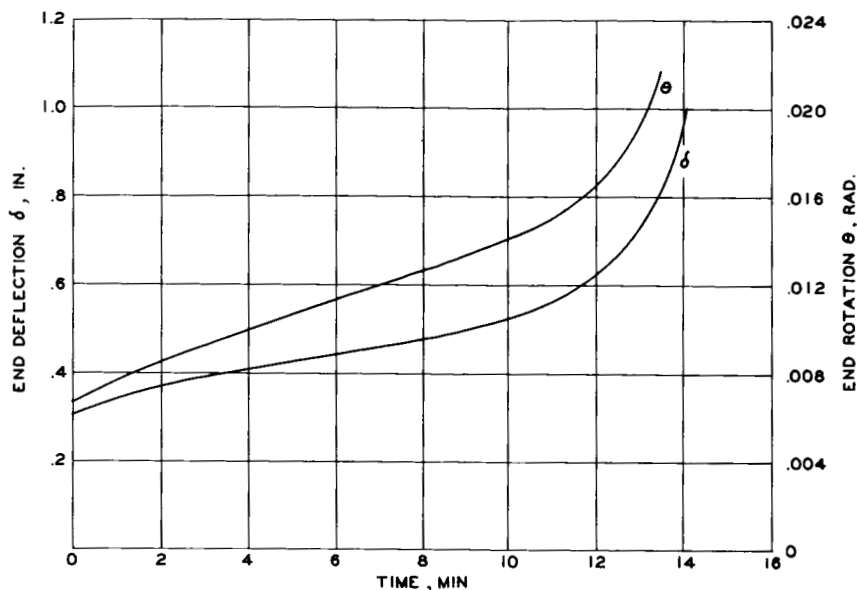
(c) External view of type F, experiment 71.



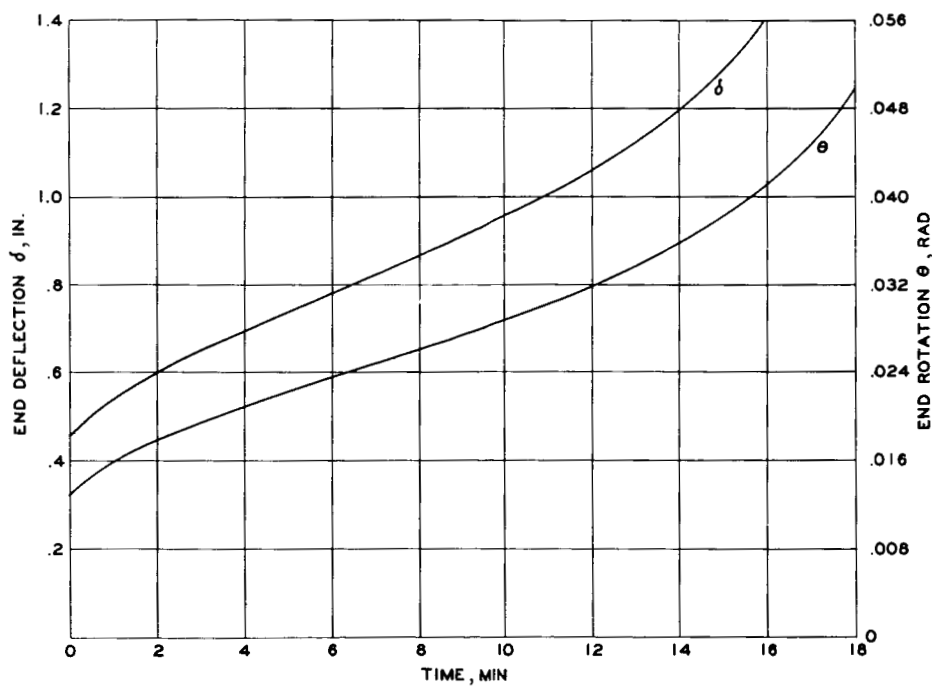
(d) Internal view of type F, experiment 71.

L-60-277

Figure 9.- Concluded.

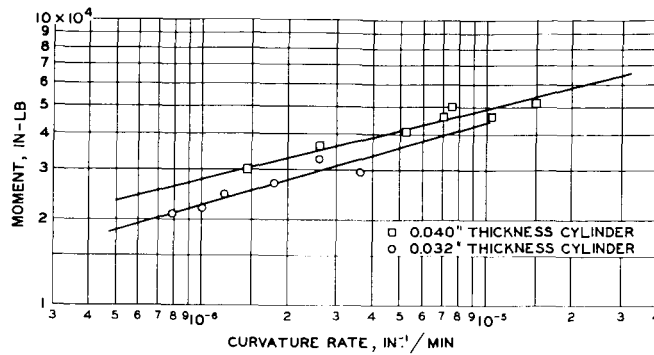


(a) Unreinforced cylinder of 0.051-inch thickness (test 17).

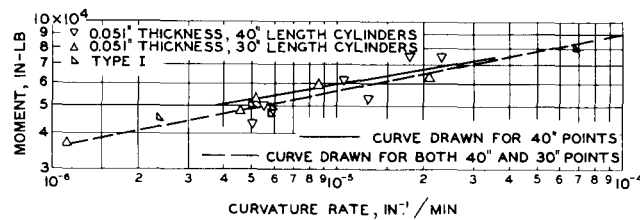


(b) Reinforced cylinder of type C (test 58).

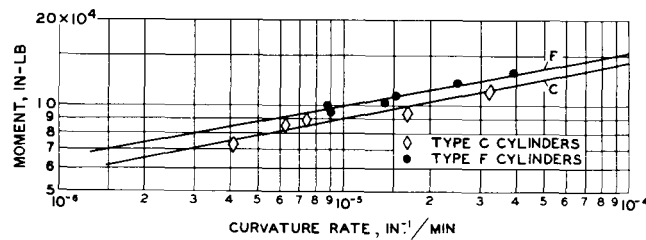
Figure 10.- Creep curves for two types of cylinders.



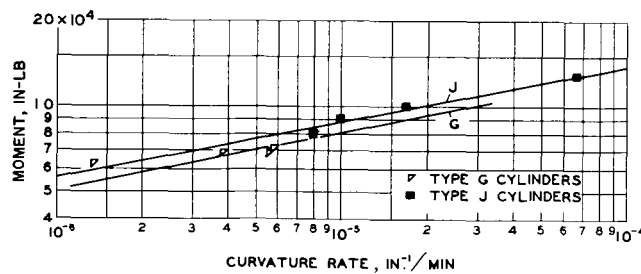
(a) 0.040- and 0.032-inch-thick cylinders.



(b) 0.051-inch-thick and type I cylinders.



(c) Type C and type F cylinders.



(d) Type G and type J cylinders.

Figure 11.- Determination of creep constants.

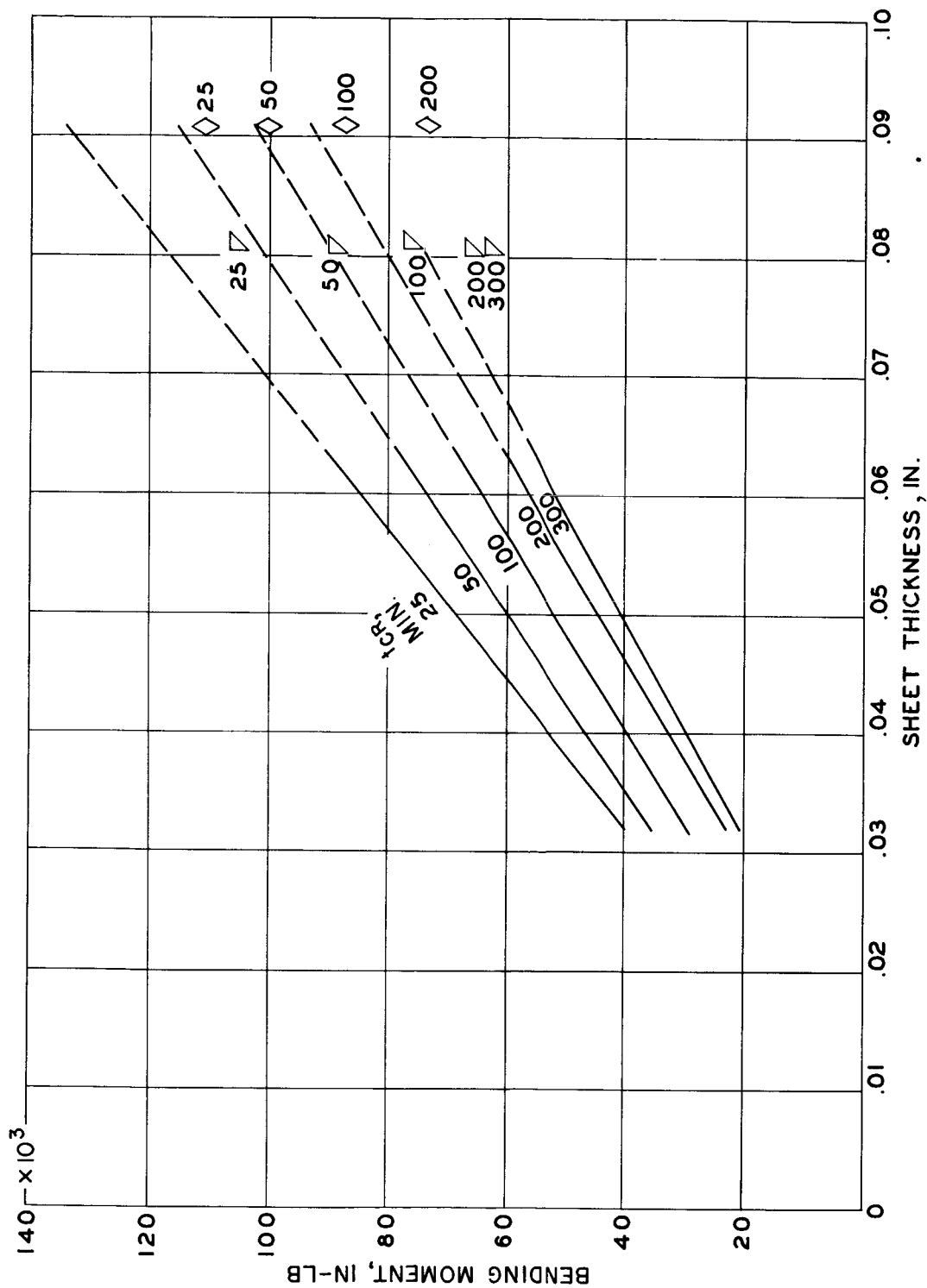


Figure 12.- Bending moment versus sheet thickness for different values of critical time.

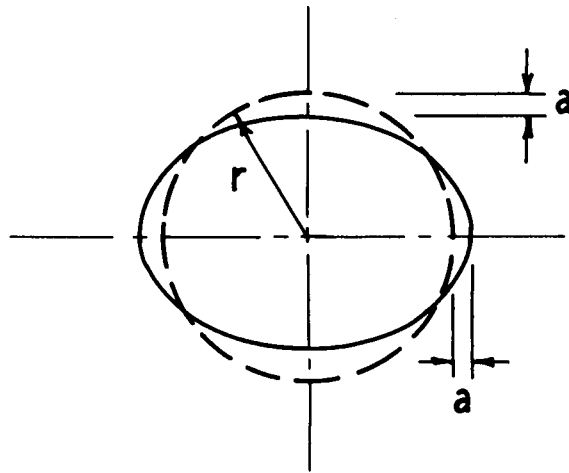
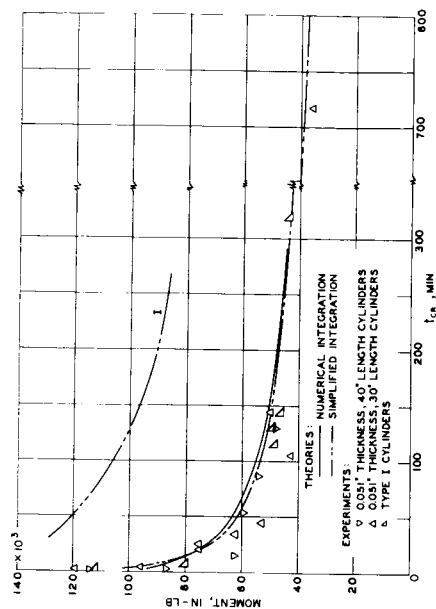
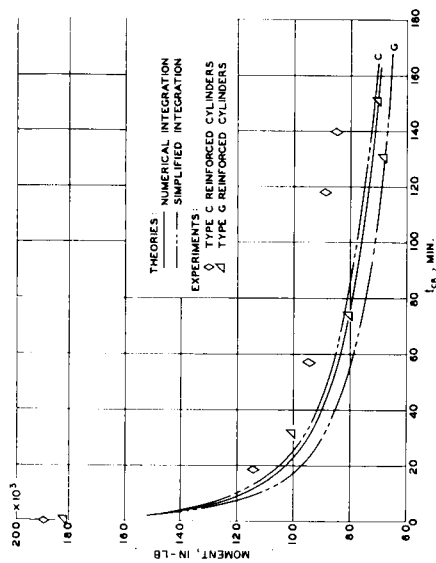


Figure 13.- Flattening of cross section.

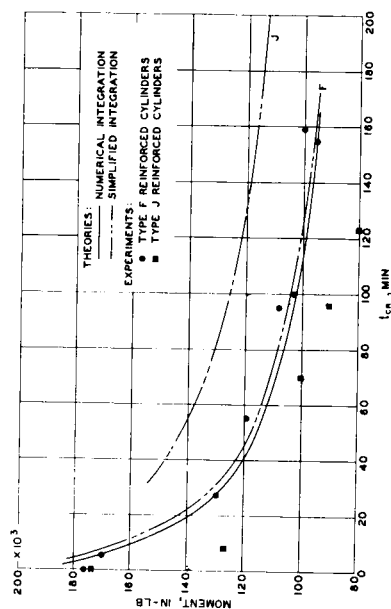


(a) Unreinforced cylinders of 0.040- and 0.032-inch thickness.

(b) Unreinforced cylinders of 0.051-inch thickness and 30- and 40-inch lengths, and type I reinforced cylinders.

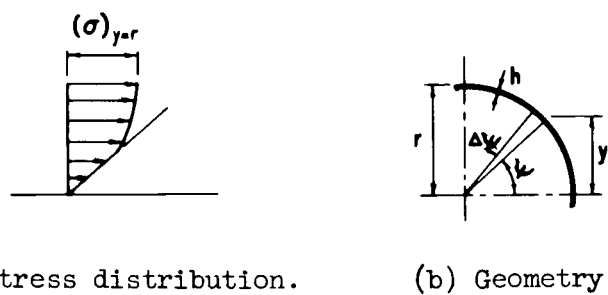


(c) Type C and G reinforced cylinders.



(d) Type F and J reinforced cylinders.

Figure 14.- Moment versus critical time for theories and experiments.



(a) Stress distribution. (b) Geometry.

Figure 15.- Cylinder cross section.

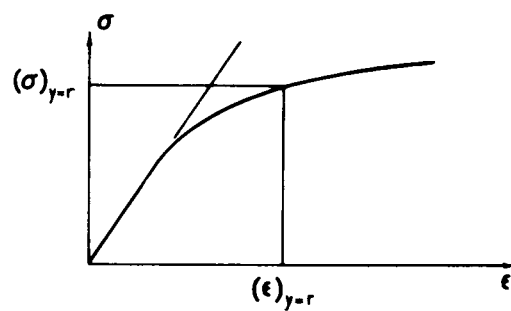


Figure 16.- Stress-strain curve of sheet material.

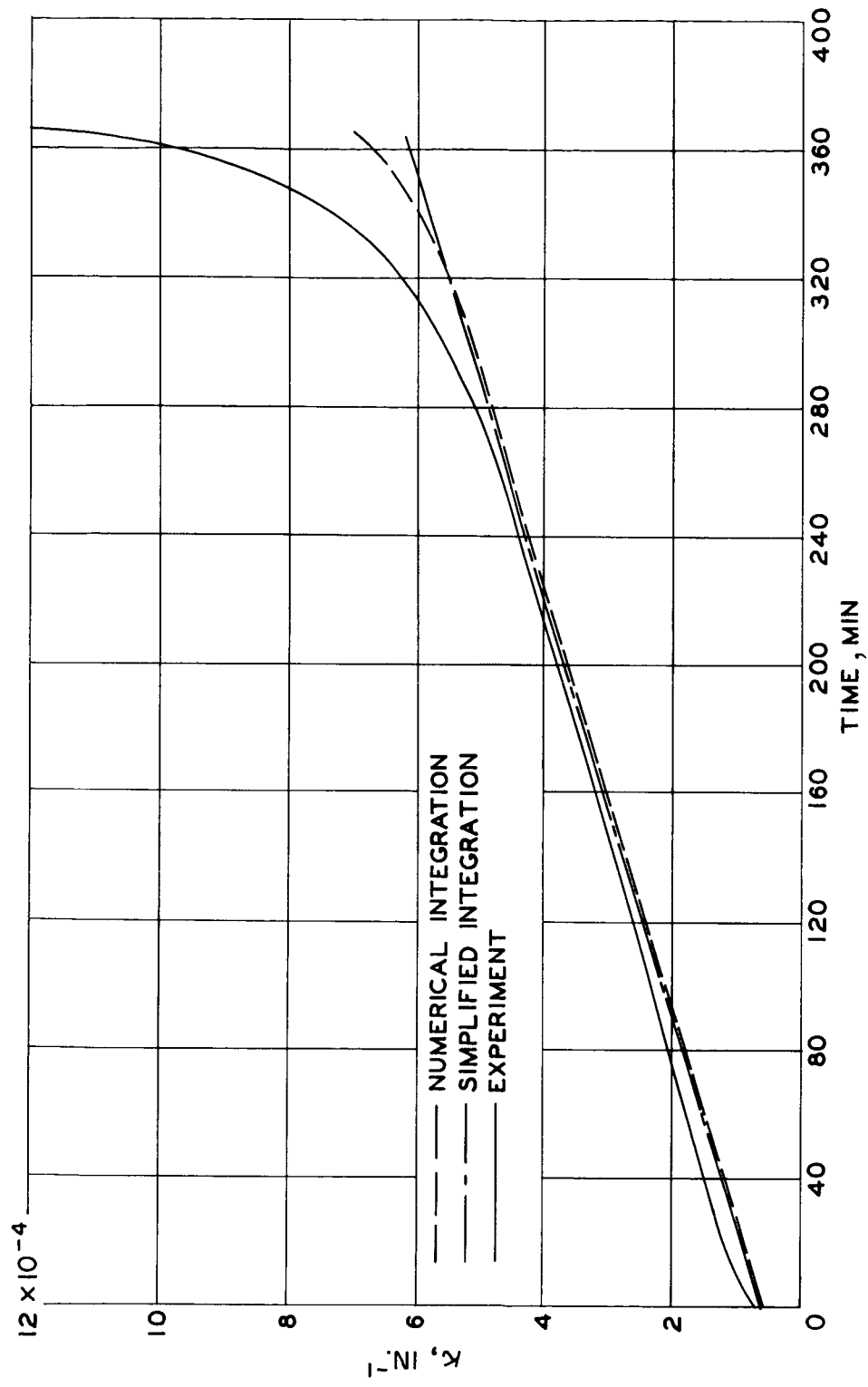


Figure 17.- Curvature versus time for theories and experiment. Test 31.